IEEE Access
Multidisciplinary ⋮ Rapid Review ⋮ Open Access Journal

Received August 16, 2019, accepted August 26, 2019, date of publication August 29, 2019, date of current version September 12, 2019.

Digital Object Identifier 10.1109/ACCESS.2019.2938409

Forward Electrocardiogram Modeling by Small Dipoles Based on Whole-Body Electric Field Analysis

TATSUHITO NAKANE[1], TAKAHIRO ITO[1], (Member, IEEE), NOBUAKI MATSUURA[2], HIROYOSHI TOGO[2], (Senior Member, IEEE), AND AKIMASA HIRATA[1], (Fellow, IEEE)

[1]Department of Electrical and Mechanical Engineering, Nagoya Institute of Technology, Nagoya 466-8555, Japan
[2]NTT Device Innovation Center, NTT Corporation, Kanagawa 243-0198, Japan

Corresponding author: Takahiro Ito (ito.t@nitech.ac.jp)

ABSTRACT Mathematical modeling of detailed cardiac function has become possible in recent years. Computer simulations have been conducted to reproduce electrical phenomena of the heart. However, substantial effort and computational cost are required to construct an electrocardiogram (ECG) generation model based on multiple parameters of cardiac tissue. In addition, most previous studies simplified the anatomy and the region of the body considered. Such modeling may not be applicable for the system design of wearable sensing in ECG. In this study, we propose a computational model of ECG generation with multiple electric dipoles to reduce the complexity and computational cost of ECG modeling. In this study, first, the electrical potential distribution on the surface of an anatomically detailed model was computed with volume conductor (electrical) analysis. We subsequently simulated the propagation of the electrical excitation of the heart by sequentially placing electric dipoles according to conduction velocity. Our computational results demonstrate the effectiveness of the ECG model using electric dipoles in comparison with measurement and the necessity to discuss the ground in a 12-lead ECG for the whole-body model. The required computational time was less than 30 min even in a workstation (2 CPUs, 28 cores, and 2.20 GHz), i.e., significantly less than those of previous studies.

INDEX TERMS Electrocardiography, electromagnetic modeling, finite difference methods.

I. INTRODUCTION

An electrocardiogram (ECG) is the recording of bioelectric signals, which are measured by multiple electrodes on a body surface, from the heart. The main feature of ECGs is that signals can be measured in a noninvasive manner and almost in real time [1]. ECGs were invented more than 100 years ago, and they are still used as an essential tool to detect early heart disease. Recently, ECG has been applied in wearable-based systems for monitoring health condition [2].

The mechanisms of cardiac electrophysiology have been elucidated by numerous *in vivo* and *in vitro* experimental studies (e.g., [1]–[3]). In recent years, improvements in computer performance have enabled detailed modeling toward clarifying these mechanisms [4]–[6].

To interpret ECG signals for medical diagnostics, computer modeling and simulation of ECGs, known as the forward problem of electrocardiography, have become essential issues [7], [8]. Several studies have been conducted as the first step to solve the inverse problem of electrocardiography [9]–[11]. The reproduction of the forward problem of electrocardiography depends on various factors such as modeling the electrical activity in the heart, the heart–body coupling condition, the conduction system, and myocardial anisotropy [12]. The important factors in the forward problem are the modeling of a cardiac source and volume conductor [12]; the latter is an electromagnetic analysis where the human tissue is assumed to be a conductor [9], [13]–[16]. Two primary approaches can be used to represent a cardiac source. One is using a representative bidomain model in which the electrical behavior at a cell is derived as a cardiac source and subsequently excitation propagation is analyzed in more detail using a volume conductor model [17]. However, this model is computationally complicated because it sets multiple parameters of cardiac tissue including conductivity tensor and membrane capacity. [17]. The other model considers an equivalent current dipole (single dipole, moving dipole, multiple dipoles, etc.) as the basic cardiac source [1], [18]–[21].

The associate editor coordinating the review of this article and approving it for publication was Lei Zhao.

Direct electrophysiological interpretation is possible only for electrical activities in a small part of the myocardium in a dipole model [18], [20].

Even though volume conductor modeling has been developed extensively, multiscale and multiphysics techniques are further required to construct gene levels and personalized cardiac models [4], [8], [22], [23]. The volume conductor model for a simplified geometric model has been widely developed to consider the anatomical structure of the heart [8]. However, to reproduce a realistic 12-lead ECG, it is necessary to analyze excitation propagations over a whole-body model. The misplacement of electrode positions has caused substantial error in clinical ECGs [24]. Moreover, the position of limb electrodes has directly affected all leads and changed the shape and amplitude of the ECG waveform [25]. However, many previous studies have only analyzed the torso part in detail, thereby simplifying the model anatomy [13], [15], [26]. To the best of our knowledge, only one study has analyzed ECGs using anatomical whole-body models but with a fixed single dipole as a preliminary study [21].

Based on the abovementioned difficulties in the forward problem of electrocardiography, it is important to reproduce ECGs using a simpler computational procedure. If an ECG is replicated in a relatively simplified manner, the resultant ECG waveform may be applicable to different fields including the inverse problems of electrocardiography and healthcare applications such as optimization of electrode positions for wearable ECG monitoring devices.

In this study, we propose a computational model of ECG generation with multiple electric dipoles. In the proposed model, the body surface potential distribution of an anatomically detailed model is computed with the volume conductor model in a frequency domain based on a quasi-static approximation. The electrophysiological phenomenon of the heart was approximated by multiple electric dipoles placed sequentially in the conduction system. Subsequently, ECG waveforms were simulated by superposing the ECG potential generated by each dipole in the time domain considering the conduction velocity of current.

II. METHOD AND MODEL

A. ANATOMICAL HUMAN BODY MODEL

We used the anatomical human model of a normal Japanese adult male (TARO) [27] to model a volume conductor. This model consists of 51 types of anatomical tissues, such as skin, muscle, bone, and heart, with a resolution of 2 mm. The heart of the model consists of only one tissue, and the atrium and ventricle are not clearly divided. The electrical conductivity of the tissues is assigned based on the 4-Cole–Cole model [28]. The skin's conductivity is assigned as 0.1 S/m [29] because extremely low conductivities have been reported by a few studies, which correspond to the stratum corneum [30].

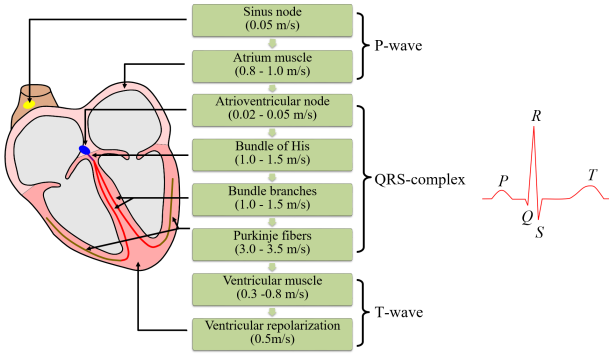

FIGURE 1. Outline of cardiac conduction system; definitions of P, Q, R, S, and T waves. The propagation speed of current reported in [1] is also shown.

B. CONDUCTION SYSTEMS OF THE HEART AND ECG

Figure 1 shows the outline of the cardiac conduction system. A sinus node, which is a crescent-shaped muscle cell, is located around the superior vena cava of the right atrium [1]. The sinus node is a self-excitable cell and generates an action potential at 60 to 100 times per minute [3]. This action potential propagates in the atrium muscle. Nonconductive walls of fibrous tissues exist at the boundary between the atrium and ventricle. In normal hearts, action potentials cannot propagate directly across the boundary. The only conduction path from the atrium to the ventricle is the atrioventricular node (A–V node) located at the atrium–ventricle boundary. After the action potential is propagated to the atrioventricular node, it is successively propagated through the bundle of His, bundle branches, and Purkinje fibers. The waveform of the ECG records a combination of electrical activities from all cardiac cells, including propagation in these specialized tissues. The typical waveform of an ECG comprises three waves: P-wave, QRS-complex, and T-wave. These waves correspond to atrial depolarization, ventricular depolarization, and repolarization, respectively. The T-wave generated by the repolarization process does not indicate the propagation of the action potential by the conduction system, and the waveform changes according to various parameters (e.g., heart rate, action potential duration, dispersion of repolarization) [31]. In addition, the primary target of this simulation is to analyze the propagation of the ECG over the whole body considering health monitoring applications. We thus do not simulate the T-wave in this study. The conduction velocity of the activation potential in each tissue is shown in Fig. 1.

We assume that the propagation of electrical excitation in the conduction pathway of the heart can be approximated by sequentially placed electric dipoles as a moving input wave source. Figure 2 shows the placement of electrical charge in the heart and the A–V node is the assumed position in the analysis model. As mentioned above, the action potential generated at the sinus node propagates throughout the atrium. Three primary specific pathways connect the sinus node to the atrioventricular node [32]. These pathways are special paths

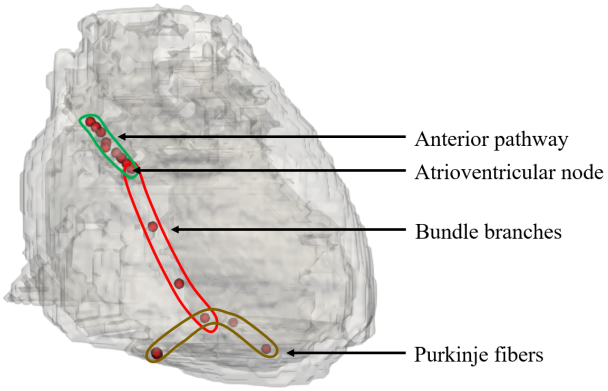

FIGURE 2. Electric charge placement patterns in the heart of anatomical model. The red dot represents the position of the electric charge.

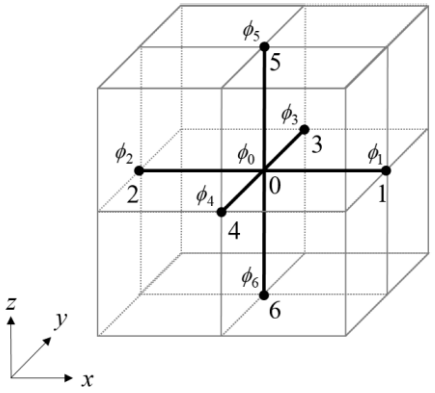

FIGURE 3. Electric scalar potential in SPFD method.

that propagate the action potential faster compared with the surrounding atrial tissues. Among them, the anterior pathway is the most prominent. Therefore, we assumed a propagation pathway only for the anterior pathway to simplify the ECG model. In addition, we simulated bundle branches by one path and Purkinje fibers by two paths. In the simulation of Purkinje fibers, we placed a single input source corresponding to each path and the result of each analysis was combined to reproduce the branch of the paths.

The length between the electric dipoles depends on the arrangement angle; thus, it is difficult to unify this length. If the amount of charge, q, and the length between the electric dipoles, $\boldsymbol{l}$, is sufficiently short relative to the distance, $\boldsymbol{r}$, from the middle point of two charges to a measurement point, the electric potential, ϕ_r generated by the electric dipole is proportional to $\boldsymbol{l}$ [1]. This is because the electric potential corresponding to the electric dipole, $\boldsymbol{P}$ of arbitrary magnitude is $\phi_r \propto \boldsymbol{P} = q\boldsymbol{l}$ based on the assumption of linearity, regardless of whether the volume conductor is homogeneous or inhomogeneous. Assuming that the action potential generated at the sinus node propagates through the cardiac tissue at a constant amplitude, which is supported by charge conservation, modeling necessary by equalizing the length between the electric dipoles. However, in the voxel model, the charge of the input source is placed only at each vertex, and it is difficult to unify the dipole moment while discretizing the current pathway. Therefore, the nonuniformity of the dipole moment is addressed by introducing a compensation factor, which is given by equation (1), for the scalar potential obtained by numerical calculation.

$$\phi_m^{'} = \phi_m \times \frac{l_{\mathrm{o}}}{l_{\mathrm{d}m}}, \tag{1}$$

where ϕ_m, l_{o}, and $l_{\mathrm{d}m}$ are the scalar potential obtained by numerical calculation, the average of the dipole length in each part, and the length of dipoles obtained in each analysis, respectively.

In this study, the frequency of the electric dipole (potential) was assumed as 1 Hz for simplicity. This is because the activation potential is generated at the sinus node in the range of 60 to 100 times per minute.

C. SCALAR-POTENTIAL FINITE-DIFFERENCE METHOD

In the ECG modeling, the displacement current can be ignored because the intrinsic frequency of the cardiac action potential is approximately 1 Hz [1], [3] (See also Sec. II. B), which is well below 100 kHz [33], which is an estimate of the regime of the quasi-static regime in biological tissues.

The numerical methods typically used for solving the forward problem of electrocardiography are the electro-quasi-static finite element method (FEM) with tetrahedrons [26]. However, the computational cost of analyzing a whole-body model using the FEM is extremely high when the model is discretized with tetrahedrons. Therefore, we solve potentials in an analysis area based on the scalar-potential finite-difference (SPFD) method, which is suitable for the fast calculation of the electric field in a frequency domain. Because of the discretization with voxels, anatomical human body models are used easily [34], [35].

The scalar potential, ϕ, induced in the volume conductor is given by the Poisson equation.

$$\begin{cases} \nabla \cdot (\sigma \nabla \phi) = -\nabla \cdot \boldsymbol{J} \text{ in } \Omega \\ (\sigma \nabla \phi) \cdot \boldsymbol{n}_B = 0 \text{ on } B_s, \end{cases} \tag{2}$$

where σ, $\boldsymbol{J}$, $\boldsymbol{n}_B$, Ω, and B_s are the electrical conductivity, current density, a unit vector outwardly normal to the body surface, volume conductor, and body surface, respectively. We discretize equation (2) based on a quasistatic approximation [36] to obtain the following equation:

$$\left(\sum_{\mathrm{n}=1}^{6} S_{\mathrm{n}}\right)\phi_0 - \sum_{\mathrm{n}=1}^{6} S_{\mathrm{n}}\phi_{\mathrm{n}} = -j\omega q, \tag{3}$$

where n, ϕ_{n}, ω, q, and S_{n} denote the node indexes, electric scalar potential at node n-th node, angular frequency, electrical charge at 0-th node, and edge conductance from the n-th node to the 0-th node derived from the tissue conductivity of the surrounding voxels, respectively. Figure 3 shows the

definition of the electric scalar potential in the SPFD method. The electric scalar potential is defined as an unknown variable on the black lattice points in Fig. 3. With the difference method, the potential of the 0-th node at the intersection of cells in Fig. 3 can be defined with respect to the potential of the node in the total six directions of the adjacent x, y and z components and the edge conductance of each direction [34], [35]. The boundary condition of equation (2) is satisfied by setting air voxels adjacent to the body surface. The amount of charge is determined to generate the amplitude of ECG of healthy subjects [37]. This amount equation (3) was set equal for all the cases to satisfy the continuity of current. The branch current flowing from one node to a neighboring node along the side of the voxels was derived by defining scalar potentials (unknowns) at each node of a cubic voxel. This branch current included a scalar potential due to the applied electric charge and the impedance between nodes. Subsequently, simultaneous equations were obtained by utilizing Kirchhoff's current law at all nodes. Potentials were solved iteratively using the successive over-relaxation (SOR) method [38] and multigrid method [39]. The SOR method solves a linear system of equations using grids of the same size. It requires considerable time to obtain sufficient accuracy. On the contrary, the multigrid method efficiently reduces errors by utilizing multiple grids of different sizes. Therefore, we prepared six multigrid levels to reduce the time required for iterative calculations and continued the calculations until the relative residual was less than 10^{-6}.

D. 12-LEAD ECG

The most typically used ECG is the standard 12-lead ECG composed of Einthoven limb leads, Goldberger augmented leads, and Wilson's precordial leads [1]. Einthoven limb leads and Goldberger augmented leads are collectively referred to as limb leads. Each lead is derived by the following equations (4):

$$\begin{aligned}
\mathrm{I1} &= \psi_\mathrm{L} - \psi_\mathrm{R} \\
\mathrm{I2} &= \psi_\mathrm{F} - \psi_\mathrm{R} \\
\mathrm{I3} &= \psi_\mathrm{F} - \psi_\mathrm{L} \\
\mathrm{aV_R} &= \psi_\mathrm{R} - (\psi_\mathrm{F} + \psi_\mathrm{L})/2 = -(\mathrm{I1} + \mathrm{I2})/2 \\
\mathrm{aV_L} &= \psi_\mathrm{L} - (\psi_\mathrm{F} + \psi_\mathrm{R})/2 = \mathrm{I1} - \mathrm{I2}/2 \\
\mathrm{aV_F} &= \psi_\mathrm{F} - (\psi_\mathrm{R} + \psi_\mathrm{L})/2 = \mathrm{I2} - \mathrm{I1}/2 \\
\mathrm{Vn} &= \psi_\mathrm{n} - (\psi_\mathrm{F} + \psi_\mathrm{R} + \psi_\mathrm{L})/3, \qquad (4)
\end{aligned}$$

where ψ_n, ψ_F, ψ_R, and ψ_L are the measurement potentials of the chest, left ankle, right wrist, and left wrist, respectively.

We selected nine electrode (observation) points corresponding to electrode positions of the standard 12-lead ECG that are located on the chest and limb of the human model. In the case of precordial leads, the average potential of both wrists and of the left ankle were considered as the reference potential (Wilson Central Terminal: WCT) [1]. Figure 4 shows the electrode positions for an ECG.

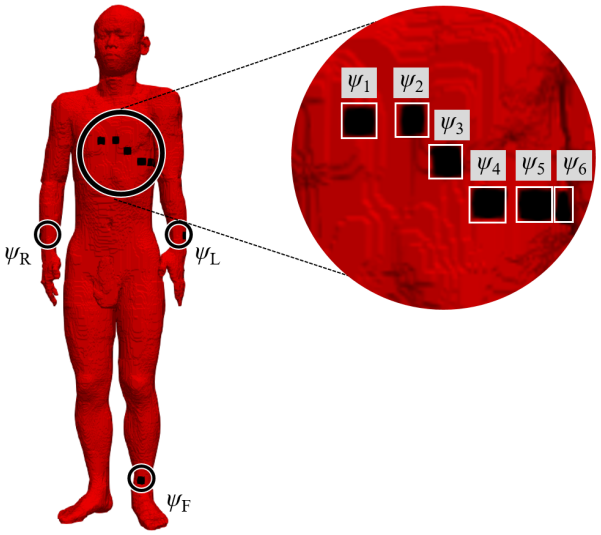

FIGURE 4. Positions of ECG electrodes.

E. RECONSTRUCTION OF ECG WAVEFORM

The ECG is reconstructed in the time domain as post-processing. Generally, sampled signals are expressed in an equal-interval time domain. However, in this study, we generated the time axis series based on signal propagation speed and the approximated continuous signal was obtained through linear interpolation. Subsequently, the ECG was reconstructed by limiting the frequency component to 100 Hz or less for each of the P-wave and QRS-complex [33]. First, the body surface potential for a single electric dipole as an input source was calculated using the SPFD method. Next, we calculated the propagation time of the action potential in the heart using its propagation velocity and the distance between positive and negative charges. The distance between positive and negative charges is determined by the direction of the electric dipole, which is based on the angle at which the conduction pathway is discretized. Then, the body surface potential distribution at the time calculated by the equations (5) and (6) is calculated. Finally, the ECG is reconstructed based on 12-lead ECG from the body surface potential distribution at each time.

The time axis series t_k at the k-th electrical charge is derived by the following equations (5) and (6).

$$t_k = \sum_{i=1}^{k} \Delta t_i, \qquad (5)$$

$$\Delta t_k = \begin{cases} \dfrac{|\boldsymbol{r}_k - \boldsymbol{r}_{k-1}|}{v_{part}} & k = 1, \ldots, m-1, m+1, \ldots \\ \text{Interval time} & k = m \end{cases} \qquad (6)$$

where r_k, v_{part}, and m are the position vector of k-th electrical charge, the propagation speed in the atrium and ventricle, and the index representing the A–V node of the analysis model, respectively. The propagation velocities in the atrium and

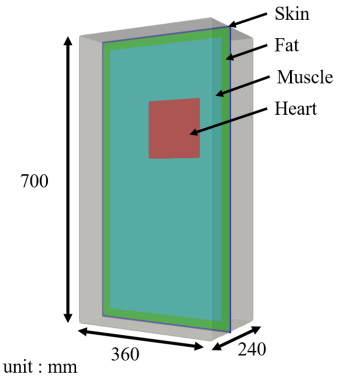

FIGURE 5. Geometry of simplified torso model.

ventricle are 0.3 and 1.9 m/s, respectively [1], [3]. Finally, the leads are integrated in the time domain.

III. COMPUTATIONAL RESULTS

A. VERIFICATION OF NUMERICAL METHODS

Computer simulation was performed to verify the numerical accuracy for the forward problem of ECG by the SPFD method. The volume conductor was approximated by a rectangular torso model consisting of 7,560,000 voxels. The torso model was solved using COMSOL Multiphysics (COMSOL AB, Switzerland, v5.3a) which is based on FEM solver with Intel Xeon E5-2643 v4 @ 3.40 GHz running Windows 10. Figure 5 shows the geometry of simplified torso model. Numerical accuracy was evaluated by relative difference (RD) defined as follows.

$$\mathrm{RD} = \frac{\frac{1}{N_\mathrm{s}}\sum_{i=1}^{N_\mathrm{s}}\left|\phi_i^{\mathrm{FEM}} - \phi_i^{\mathrm{SPFD}}\right|}{\frac{1}{N_s}\sum_{i=1}^{N_\mathrm{s}}\left|\phi_i^{\mathrm{SPFD}}\right|} \times 100, \tag{7}$$

where ϕ^{FEM}, ϕ^{SPFD}, and N_s are the scalar potential obtained by FEM and SPFD, and number of skin elements. The same multigrid levels and relative residuals were set as in Sec. II C to compare numerical accuracy.

Figure 6 shows the RD between FEM and SPFD with increasing number of tetrahedral elements. Table 1 shows numerical accuracy and CPU time between FEM and SPFD. Table 1 shows that SPFD is about 5 times faster than FEM when RD is less than 1%. More pronounced differences in computational costs would be observed for more complex phantoms. Figure 7 shows the surface potential distribution from SPFD and FEM in simplified torso model.

B. DEMONSTRATION OF MODEL

Figure 8 shows the computed distribution of the body surface potential corresponding to different electric dipoles. As shown in Fig. 8(a), the body surface potential distributions differ significantly for different dipoles. Figure 9 shows the

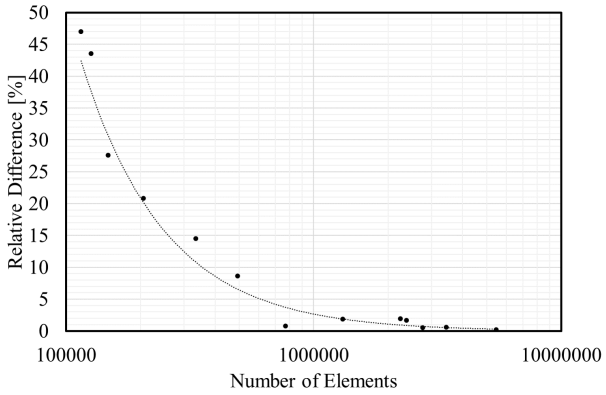

FIGURE 6. Relative difference of scalar potential computed with FEM and SPFD. The fitted curve was obtained by power approximation ($y = \alpha x^{\beta}$). $\alpha = 1.27 \times 10^8$, $\beta = -1.28$ and coefficient of determination was 0.91.

TABLE 1. Summary of computational efficiency and numerical accuracy between FEM and SPFD in simplified torso model.

	Number of Elements	RD [%]	CPU time [s]
FEM	115007	47.0	3
	126022	43.5	4
	147631	27.6	5
	205800	20.8	8
	333845	14.5	11
	492305	8.6	14
	769171	0.8	21
	1308803	1.9	34
	2240546	1.9	62
	2368529	1.7	66
	2762802	0.5	83
	3427523	0.6	108
	5462296	0.2	181
SPFD	7560000	-	3.859

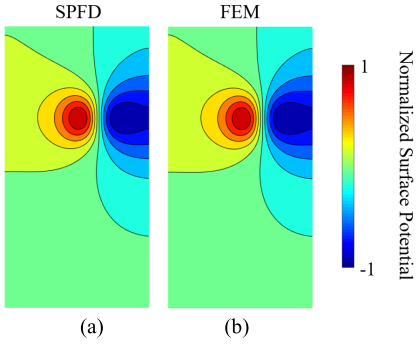

FIGURE 7. Surface potential distribution from SPFD and FEM in simplified torso model. (a) Consists of 7560000 voxels. (b) Consists of 769171 tetrahedrons.

12-lead ECG reconstructed as the waveform of the ECG in terms of Sec. II E. Figure 10 shows the change in the WCT potential.

C. VALIDATION

The characteristics of the waveform of the P-wave and QRS-complex are different depending on each lead [40], [41]. The polarity of the P-wave is always positive in leads I1,

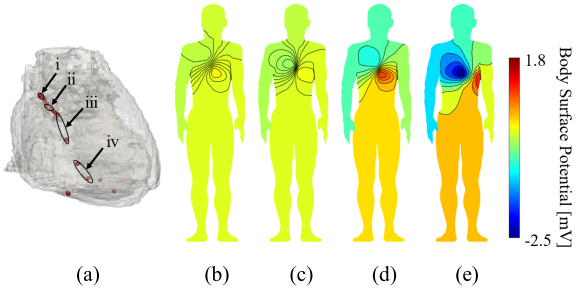

FIGURE 8. (a) Electric dipoles. (b), (c), (d), (e) are the computed body surface potential distributions corresponding to (i), (ii), (iii), and (iv), respectively.

TABLE 2. Typical amplitude and duration of ECG (measurement) reported in [37].

	Typical Amplitude and Duration	Computed Value
P-wave	≤ 0.25 mV	Maximum = 0.24 mV in V2
R-wave	≤ 1.6 mV	Maximum = 1.4 mV in V6
P-wave interval	0.11 s	0.11 s
QRS interval	0.09 s	0.08 s

I2, aV_F and from V3 to V6, and it is negative only in lead aV_R. It is variable in leads I3, aV_L and V1-V2. In addition, the P-wave in lead V1 exhibits biphasicity with positive and negative deflection. In Einthoven limb leads, the polarity of the QRS-complex waveform is positive in leads I1 and I2, and is positive, negative, or intermediate in lead I3. In Goldberger augmented leads, the polarity of the QRS-complex waveform is negative in lead aV_R and positive or intermediate in leads aV_L and aV_F.

In precordial leads, the polarity of the QRS-complex waveform is negative in leads V1 and V2 and positive in leads V5 and V6. It is positive, negative, or intermediate in leads V3 and V4. The change in polarity of the QRS-complex between V3 and V4 is referred to as the transition zone. QRS-complex in precordial leads are assessed qualitatively by confirming the progression of the R wave, which is an important property in precordial leads [14]. Figure 11 shows the R-wave progression in precordial leads. In addition to the polarity of these waveforms, the ECG records the waveform duration and its amplitude as important information, and previous study have used these feature quantities as validation [37]. Table 2 shows the comparison of the amplitude and duration of the reported ECG with those of a previous study [37].

As shown in Fig. 9, the approximate form of the P-wave is reproduced at all lead points. The duration of the P-wave matches the typical values in Table 2. Furthermore, the amplitude of the P wave is within the typical upper and lower value of 0.05 mV to 0.25 mV [41].

Therefore, it is sufficient to simulate the action potential in the atrium only with the anterior pathway. Moreover, the approximate form of the QRS-complex can be reproduced and the maximum value of the R-wave is within the range of normal values at all lead points. The duration of the QRS-complex indicates an appropriate value. Furthermore, as

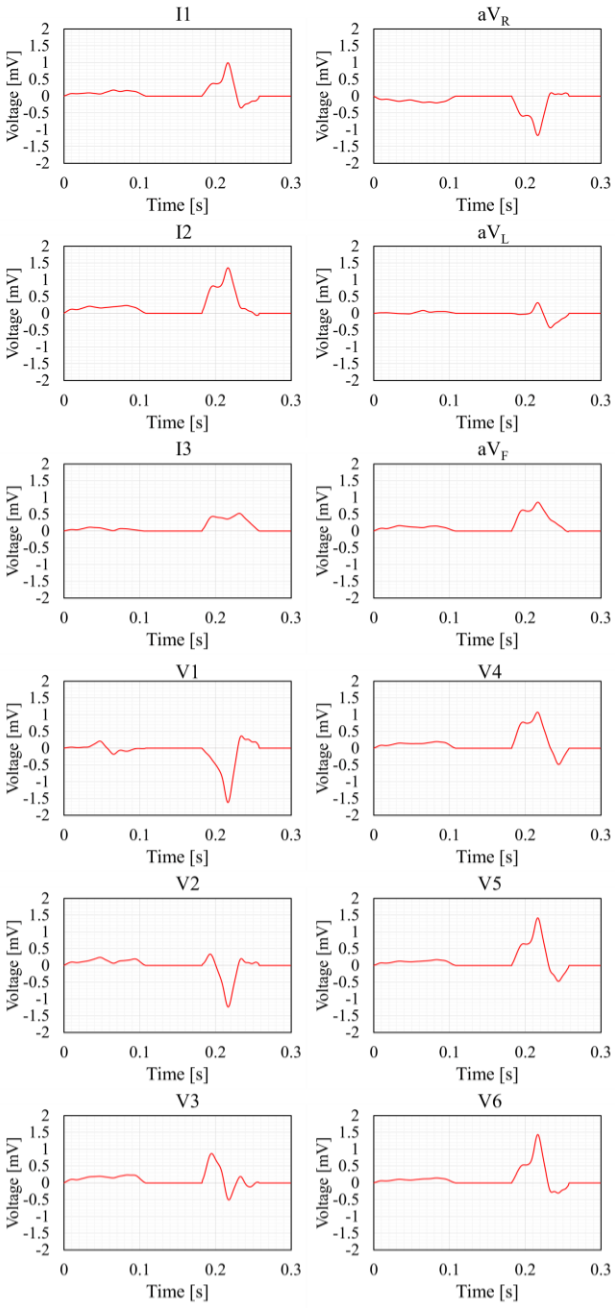

FIGURE 9. Computed induced voltage at the electrodes of the standard 12-lead ECG.

shown in Fig. 11 the transition zone that is characteristic of precordial leads and progression of R-wave can be confirmed.

As shown in Fig. 10, the form of change in the WCT potential is similar to that of the 12-lead ECG. The order of 0.2 mV amplitude of the WCT potential is consistent with that obtained in a previous study [25].

D. ELECTRODE POSITION DEPENDENCY

We investigated whether electrode position affected the constructed ECG signals. Figure 8 shows that no difference

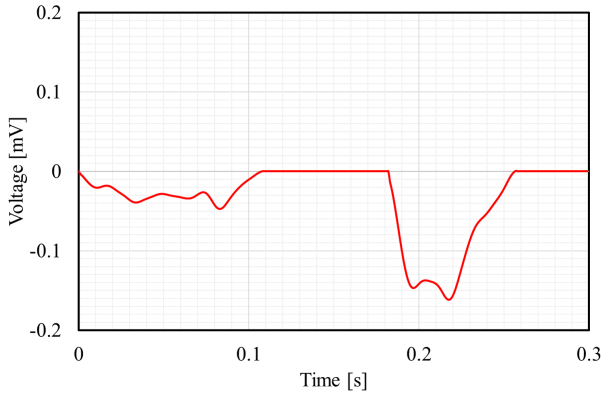

FIGURE 10. Change in WCT potential during 12-lead ECG reconstruction.

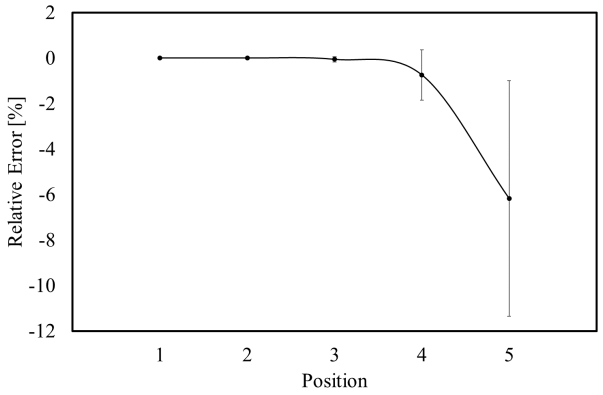

FIGURE 13. Relative error in I1 at each measurement position.

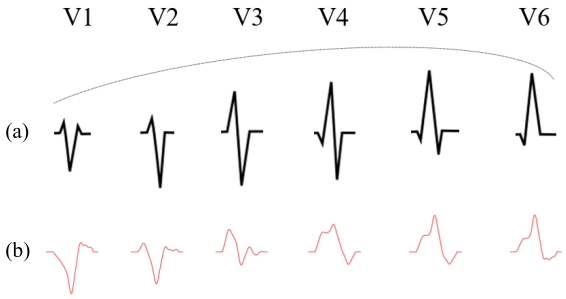

FIGURE 11. Confirmation of R-wave progression in precordial leads. (a) Typical waveform from [40]. (b) Computed one.

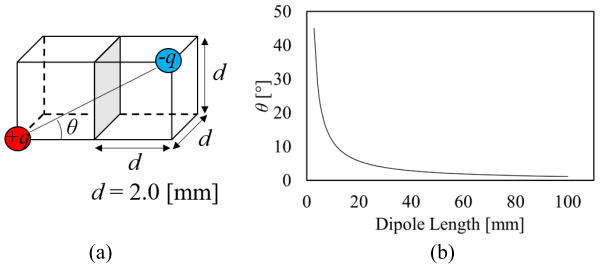

FIGURE 14. (a) Input source arrangement when the dipole length is $\sqrt{20}$ mm. (b) Angular resolution with respect to dipole length of input wave source.

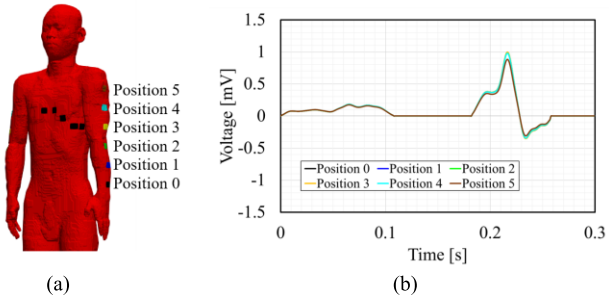

FIGURE 12. (a) Measurement positions on the left arm. (b) Variation in I1 at each position.

exists between the magnitudes of potential from the wrist to the shoulder. Even if the electrode position of a limb shifts by several centimeters, the effect on the ECG waveform can be expected to be marginal. However, as mentioned in Section I, the position of the limb electrode has been reported to affect the shape and amplitude of the ECG [25]. Hence, we examined the variation in the ECG by changing the electrode positions on both arms from the wrist to the shoulder. Figure 12 shows the measurement positions on the left arm (and the right arm) and the variation in I1 at each position. Figure 13 shows the relative error in I1 with reference to the measured potential (Position 0) on the wrist. The error bar is the standard deviation of the relative error at each potential required to construct the waveform.

IV. DISCUSSION

We proposed a new and simple ECG generation model using multiple electric dipoles considering a human whole-body model. The feature of our model was that, unlike previous studies [14], [15], [42], the electrical potential over the entire body could be computed easily with relatively low computational cost. The average computational time required for each dipole was approximately 100 s with Intel Xeon Gold-5120 @2.20 GHz running CentOS 7.5, and the total computation time of the simulation was 25 min. The post-processing time for generating the waveform was negligible. This computational cost was considerably lower compared to conventional models. For example, the UT-Heart simulator required approximately 1 day to perform computation using a supercomputer, with the consideration of substantial physiology [6].

As shown in Fig. 8, the potential distribution on the body changed depending on the position and direction of the electric dipoles. The reconstructed waveforms were well within the reference values at different electrodes. Furthermore, it has been reported that the waveform and amplitude of the WCT changed with time, as reported in an experimental study [25]. The electrode positions of precordial leads were shown to be essential because the potential differed

considerably at the chest position. In fact, the electrode positions for ECGs are carefully determined even in clinical practice. On the contrary, the body-surface potential distribution was almost identical for cases where the electrodes were located from the wrist to the arm. According to Figs. 12 and 13, changing the measurement position on both arms did not affect the ECG. However, the relative error and standard deviation increased remarkably at the measurement position above the elbow. Therefore, errors that affect the ground in a 12-lead ECG should be considered in computer simulations involving a torso model.

In the forward problem of electrocardiography, it is necessary to analyze potential using a volume conductor model with the consideration of cardiac geometry and electrode positions. The most uncertain factor is the discretization of the current pathway in a stair-casing grid. Stair-casing discretization is necessary in the finite difference method, including the SPFD method. Some of the differences in the modeling are attributable to the definition of electric dipoles, namely, the discretized input sources. In the SPFD method, dipole direction is affected by the resolution of a voxel. When assuming an extremely small dipole for discretizing the current pathway, the angle of the dipole is evidently different. For example, for a dipole with two voxels that correspond to 4 mm, which is twice the resolution of the analysis model in our computation, the dipole direction differed by the azimuth angle $= 24°$ and polar angle $= 27°$ at the maximum, resulting in an amplitude difference of 0.22 mV. This variation corresponds to the amplitude of the P-wave. In addition, as shown in Figure 14, the angular resolution in the input wave source depends on the length of the dipoles and is a tradeoff with the time resolution in the reconstruction of the waveform. This is because each pole is located on the vertex of the voxels. Thus, the dipole moment of the input sources must be compensated. This issue may not be resolved easily even if using the FEM unless the source definition is designed carefully.

In this study, we focused on analyzing the propagation of ECG over the whole body. In the future, it will be possible to reproduce the ECG by correcting the individual difference, once a detailed individual whole-body model is constructed (see, e.g., [43], [44] for the head modeling). Additional requirements for localizing the current source in the inverse problem would be accurate modeling techniques such as the creation of a personalized model and segmentation of the heart region [23], [45].

V. CONCLUSION

In this study, we proposed a new ECG generation model that considers the whole-body model with relatively low computational cost. We confirmed the effectiveness of the new computational method by comparing typical values of the ECG between the results obtained using the proposed method and the measurements in a healthy person. The computational time required for this computation was less than 30 min, which was much shorter than the conventional method even considering the whole body. In addition, we illustrated through computer simulations that the ground electrode location affected the ECG waveform when the electrodes were located above the elbow. In some cases, the whole-body model must be considered for ECG waveform construction. In the future, we will apply the proposed method to various fields such as the inverse problems of electrocardiography and healthcare applications.

REFERENCES

[1] J. Malmivuo and R. Plonsey, *Bioelectromagnetism: Principles and Applications of Bioelectric and Biomagnetic Fields*. New York, NY, USA: Oxford University Press, 1995.
[2] T. Martin, E. Jovanov, and D. Raskovic, "Issues in wearable computing for medical monitoring applications: A case study of a wearable ECG monitoring device," in *Proc. 4th Int. Symp. Wearable Comput.*, 2000, pp. 43–49.
[3] R. E. Klabunde, *Cardiovascular Physiology Concepts*, 2nd ed. Philadelphia, PA, USA: Lippincott Williams & Wilkins/Wolters Kluwer, 2012.
[4] D. Noble, "Modeling the heart–from genes to cells to the whole organ," *Science*, vol. 295, no. 5560, pp. 1678–1682, Mar. 2002.
[5] J. Lee, S. Niederer, D. Nordsletten, I. Le Grice, B. Smail, D. Kay, and N. Smith, "Coupling contraction, excitation, ventricular and coronary blood flow across scale and physics in the heart," *Philos. Trans. Roy. Soc. A, Math., Phys. Eng. Sci.*, vol. 367, no. 1896, pp. 2311–2331, Jun. 2009.
[6] S. Sugiura, T. Washio, A. Hatano, J. Okada, H. Watanabe, and T. Hisada, "Multi-scale simulations of cardiac electrophysiology and mechanics using the University of Tokyo heart simulator," *Prog. Biophys. Mol. Biol.*, vol. 110, nos. 2–3, pp. 380–389, Nov. 2012.
[7] O. Dössel, M. W. Krueger, F. M. Weber, M. Wilhelms, and G. Seemann, "Computational modeling of the human atrial anatomy and electrophysiology," *Med. Biol. Eng. Comput.*, vol. 50, no. 8, pp. 773–799, Aug. 2012.
[8] A. Lopez-Perez, R. Sebastian, and J. M. Ferrero, "Three-dimensional cardiac computational modelling: Methods, features and applications," *Biomed. Eng. Online*, vol. 14, no. 1, p. 35, Dec. 2015.
[9] M. Boulakia, S. Cazeau, M. A. Fernández, J.-F. Gerbeau, and N. Zemzemi, "Mathematical modeling of electrocardiograms: A numerical study," *Ann. Biomed. Eng.*, vol. 38, no. 3, pp. 1071–1097, Mar. 2010.
[10] B. He, G. Li, and X. Zhang, "Noninvasive imaging of cardiac transmembrane potentials within three-dimensional myocardium by means of a realistic geometry anisotropic heart model," *IEEE Trans. Biomed. Eng.*, vol. 50, no. 10, pp. 1190–1202, Oct. 2003.
[11] B. He, G. Li, and X. Zhang, "Noninvasive three-dimensional activation time imaging of ventricular excitation by means of a heart-excitation model," *Phys. Med. Biol.*, vol. 47, no. 22, pp. 4063–4078, 2002.
[12] G. T. Lines, M. L. Buist, P. Grottum, A. J. Pullan, J. Sundnes, and A. Tveito, "Mathematical models and numerical methods for the forward problem in cardiac electrophysiology," *Comput. Vis. Sci.*, vol. 5, no. 4, pp. 215–239, Apr. 2002.
[13] M. Potse, B. Dubé, and A. Vinet, "Cardiac anisotropy in boundary-element models for the electrocardiogram," *Med. Biol. Eng. Comput.*, vol. 47, no. 7, pp. 719–729, Jul. 2009.
[14] E. Schenone, A. Collin, and J.-F. Gerbeau, "Numerical simulation of electrocardiograms for full cardiac cycles in healthy and pathological conditions," *Int. J. Numer. Method. Biomed. Eng.*, vol. 32, no. 5, May 2016, Art. no. e02744.
[15] S. Sovilj, R. Magjarević, N. H. Lovell, and S. Dokos, "A simplified 3D model of whole heart electrical activity and 12-lead ECG generation," *Comput. Math. Methods Med.*, vol. 2013, Apr. 2013, Art. no. 134208.
[16] J. Okada, S. Sugiura, and T. Hisada, "Modeling for cardiac excitation propagation based on the Nernst–Planck equation and homogenization," *Phys. Rev. E, Stat. Phys. Plasmas Fluids Relat. Interdiscip. Top.*, vol. 87, no. 6, Jun. 2013, Art. no. 062701.
[17] B. J. Roth and J. P. Wikswo, "Electrical stimulation of cardiac tissue: A bidomain model with active membrane properties," *IEEE Trans. Biomed. Eng.*, vol. 41, no. 3, pp. 232–240, Mar. 1994.
[18] G.-F. Shou, L. Xia, H. L. Duan, and M. Qian, "Towards the cardiac equivalent source models in electrocardiography and magnetocardiography: A simulation study," in *Proc. Comput. Cardiol.*, Sep. 2010, pp. 859–862.

[19] G.-F. Shou, L. Xia, P. Ma, F.-K. Tang, and L. Dai, "Simulation study of a magnetocardiogram based on a virtual heart model: Effect of a cardiac equivalent source and a volume conductor," *Chin. Phys. B*, vol. 20, no. 3, Mar. 2011, Art. no. 030702.

[20] A. Van Oosterom, "Source models in inverse electrocardiography," *Int. J. Bioelectromagn.*, vol. 5, no. 1, pp. 211–214, Jan. 2003.

[21] H. J. Visser, "Taking ECG-signals from a human voxel model," in *Proc. Loughborough Antennas Propag. Conf. (LAPC)*, Nov. 2015, pp. 1–5.

[22] N. A. Trayanova, "Whole-heart modeling: Applications to cardiac electrophysiology and electromechanics," *Circ. Res.*, vol. 108, no. 1, pp. 113–128, Jan. 2011.

[23] S. Giffard-Roisin, T. Jackson, L. Fovargue, J. Lee, H. Delingette, R. Razavi, N. Ayache, and M. Sermesant, "Noninvasive personalization of a cardiac electrophysiology model from body surface potential mapping," *IEEE Trans. Biomed. Eng.*, vol. 64, no. 9, pp. 2206–2218, Sep. 2017.

[24] P. Kligfield, L. S. Gettes, J. J. Bailey, R. Childers, B. J. Deal, E. W. Hancock, G. Van Herpen, J. A. Kors, P. Macfarlane, D. M. Mirvis, and O. Pahlm, "Recommendations for the standardization and interpretation of the electrocardiogram: Part I: The electrocardiogram and its technology a scientific statement from the American heart association electrocardiography and arrhythmias committee, council on clinical cardiology; The American college of cardiology foundation; And the heart Rhythm society endorsed by the international society for computerized electrocardiology," *J. Amer. College Cardiol.*, vol. 49, no. 10, pp. 1109–1127, Mar. 2007.

[25] G. D. Gargiulo, "True unipolar ECG machine for wilson central terminal measurements," *Biomed Res. Int.*, vol. 2015, pp. 1–7, Oct. 2015, Art. no. 586397.

[26] A. V. Shahidi and P. Savard, "Forward problem of electrocardiography: Construction of human torso models and field calculations using finite element method," *Med. Biol. Eng. Comput.*, vol. 32, no. S1, pp. S25–S33, Jul. 1994.

[27] T. Nagaoka, S. Watanabe, K. Sakurai, E. Kunieda, S. Watanabe, M. Taki, and Y. Yamanaka, "Development of realistic high-resolution whole-body voxel models of Japanese adult males and females of average height and weight, and application of models to radio-frequency electromagnetic-field dosimetry," *Phys. Med. Biol.*, vol. 49, no. 1, pp. 1–15, 2004.

[28] S. Gabriel, R. W. Lau, and C. Gabriel, "The dielectric properties of biological tissues: III. Parametric models for the dielectric spectrum of tissues," *Phys. Med. Biol.*, vol. 41, no. 11, pp. 2271–2293, 1996.

[29] R. Kavet, T. Dovan, and J. P. Reilly, "The relationship between anatomically correct electric and magnetic field dosimetry and published electric and magnetic field exposure limits," *Radiat. Prot. Dosimetry*, vol. 152, no. 4, pp. 279–295, May 2012.

[30] J. Motogi, Y. Sugiyama, I. Laakso, A. Hirata, K. Inui, M. Tamura, and Y. Muragaki, "Why intra-epidermal electrical stimulation achieves stimulation of small fibres selectively: A simulation study," *Phys. Med. Biol.*, vol. 61, no. 12, pp. 4479–4490, 2016.

[31] D. di Bernardo, P. Langley, and A. Murray, "Effect of changes in heart rate and in action potential duration on the electrocardiogram T wave shape," *Physiol. Meas.*, vol. 23, no. 2, pp. 355–364, Mar. 2002.

[32] J. Merideth and J. L. Titus, "The anatomic atrial connections between sinus and A-V node," *Circulation*, vol. 37, no. 4, pp. 566–579, Apr. 1968.

[33] E. Nemati, M. J. Deen, and T. Mondal, "A wireless wearable ECG sensor for long-term applications," *IEEE Commun. Mag.*, vol. 50, no. 1, pp. 36–43, Jan. 2012.

[34] T. W. Dawson and M. Stuchly, "Analytic validation of a three-dimensional scalar-potential finite-difference code for low-frequency magnetic induction," *Appl. Comput. Electromagn. Soc. J.*, vol. 11, no. 3, pp. 72–81, 1996.

[35] P. J. Dimbylow, "Induced current densities from low-frequency magnetic fields in a 2 mm resolution, anatomically realistic model of the body," *Phys. Med. Biol.*, vol. 43, no. 2, pp. 221–230, Feb. 1998.

[36] A. Hirata, F. Ito, and I. Laakso, "Confirmation of quasi-static approximation in SAR evaluation for a wireless power transfer system," *Phys. Med. Biol.*, vol. 58, no. 17, pp. N241–N249, Sep. 2013.

[37] C. Saritha, V. Sukanya, and Y. N. Murthy, "ECG signal analysis using wavelet transforms," *Bulg. J. Phys.*, vol. 35, no. 1, pp. 68–77, Feb. 2008.

[38] A. Hadjidimos, "Successive overrelaxation (SOR) and related methods," *J. Comput. Appl. Math.*, vol. 123, nos. 1–2, pp. 177–199, Nov. 2000.

[39] I. Laakso and A. Hirata, "Fast multigrid-based computation of the induced electric field for transcranial magnetic stimulation," *Phys. Med. Biol.*, vol. 57, no. 23, pp. 7753–7765, 2012.

[40] R. J. Prineas, R. S. Crow, and Z.-M. Zhang, *The Minnesota Code Manual of Electrocardiographic Findings*, 2nd ed. London, U.K.: Springer-Verlag, 2010.

[41] A. R. Pérez-Riera, L. C. de Abreu, R. Barbosa-Barros, J. Grindler, A. Fernandes-Cardoso, and A. Baranchuk, "P-wave dispersion: An update," *Indian Pacing Electrophysiol. J.*, vol. 16, no. 4, pp. 126–133, Jul. 2016.

[42] M. A. Fernández and N. Zemzemi, "Decoupled time-marching schemes in computational cardiac electrophysiology and ECG numerical simulation," *Math. Biosci.*, vol. 226, no. 1, pp. 58–75, Jul. 2010.

[43] M. Parazzini, S. Fiocchi, A. Cancelli, C. Cottone, I. Liorni, P. Ravazzani, and F. Tecchio, "A computational model of the electric field distribution due to regional personalized or nonpersonalized electrodes to select transcranial electric stimulation target," *IEEE Trans. Biomed. Eng.*, vol. 64, no. 1, pp. 184–195, Jan. 2017.

[44] S. Aonuma, J. Gomez-Tames, I. Laakso, A. Hirata, T. Takakura, M. Tamura, and Y. Muragaki, "A high-resolution computational localization method for transcranial magnetic stimulation mapping," *NeuroImage*, vol. 172, pp. 85–93, May 2018.

[45] G. Li and B. He, "Localization of the site of origin of cardiac activation by means of a heart-model-based electrocardiographic imaging approach," *IEEE Trans. Biomed. Eng.*, vol. 48, no. 6, pp. 660–669, Jun. 2001.

TATSUHITO NAKANE received the B.E. degree in electrical and electronic engineering from the Nagoya Institute of Technology, Nagoya, Japan, in 2018, where he is currently pursuing the master's degree in electrical and mechanical engineering.

His current research interests include biological signal propagation and healthcare applications.

TAKAHIRO ITO received the B.E., M.E., and Ph.D. degrees from the Nagoya Institute of Technology, Aichi, Japan, in 2013, 2015, and 2017, respectively, where he has been an Assistant Professor with the Graduate School of Engineering, since April 2017. He has involved in the research of computational electromagnetics in biology and medical applications.

NOBUAKI MATSUURA received the B.S. degree in applied physics and the M.E. degree in energy science from the Tokyo Institute of Technology, in 1990 and 1992, respectively. He joined NTT, in 1992. He is currently a Senior Research Engineer with the NTT Device Innovation Center.

HIROYOSHI TOGO (SM'11) received the M.Sc. and Ph.D. degrees in applied physics and electronic engineering from the University of Tsukuba, Ibaraki, Japan, in 1996 and 2010, respectively. He joined Musashino Opto-Electronics Laboratories, Nippon Telegraph and Telephone Corporation (NTT), in 1996. From 1996 to 2001, he was involved in the development of the thermo-capillary waveguide-based optical switch, and from 2001 to 2002, he endeavored to commercialize it for NTT Electronics Inc. Since 2002, he has been researching ultrawideband impulse radio systems using photonic techniques and millimeter-wave tomography with electro-optic probing, and is currently a Senior Research Engineer with NTT Microsystem Integration Laboratories, Kanagawa, Japan.

Dr. Togo is a member of the IEEE Photonics Society, the IEEE Antenna and Propagation Society, the IEEE Microwave Theory and Techniques Society (MTT-S), and the Institute of Electronics, Information and Communication Engineers of Japan. He was a recipient of the 2006 Asia–Pacific Microwave Photonics Conference AP-MWP Award and the 2010 European Conference on Antenna and Propagation Award.

AKIMASA HIRATA (S'98–M'01–SM'10–F'17) received the B.E., M.E., and Ph.D. degrees in communications engineering from Osaka University, Suita, Japan, in 1996, 1998, and 2000, respectively. From 1999 to 2001, he was a Research Fellow of the Japan Society for the Promotion of Science and also a Visiting Research Scientist with the University of Victoria, Victoria, BC, Canada, in 2000. In 2001, he joined the Department of Communications Engineering, Osaka University, as an Assistant Professor. In 2004, he joined the Nagoya Institute of Technology as an Associate Professor, where he is currently a Full Professor (Chair of Electrical and Electronic Engineering, since 2018) and the Director of the Center of Biomedical Physics and Information Technology. His research interests include electromagnetics and thermodynamics in biological tissues, EMC and EMI, computational techniques in electromagnetics, and public health engineering.

Prof. Hirata is a Fellow of the Institute of Physics and IEICE, and a member of the IEE Japan and the Bioelectromagnetics Society. He is an Editorial Board Member of *Physics in Medicine and Biology*, a member of the main commission, the Chair of the project group of the International Commission on Non-Ionizing Radiation Protection, a member of the Administrative Committee, the Subcommittee (EMF Dosimetry Modeling) Chair of the IEEE International Committee on Electromagnetic Safety, and an Expert of the World Health Organization. He has received several awards, including the Young Scientists' Prize, in 2006, the Prizes for Science and Technology (Research Category 2011 and Public Understanding Promotion Category 2014) from the Commendation for Science and Technology by the Minister of Education, Culture, Sports, Science, and Technology, Japan, the IEEE EMC-S Technical Achievement Award, in 2015, the Japan Academy Medal (Best Mid-Career Award in Japan), and the JSPS Prize, in 2018. He is an Associate Editor of the IEEE TRANSACTIONS ON ELECTROMAGNETIC COMPATIBILITY. From 2006 to 2012, he was an Associate Editor of the IEEE TRANSACTIONS ON BIOMEDICAL ENGINEERING. Based on his accomplishments, he has appeared on television programs more than 100 times and in newspapers more than 1000 times, especially in East Asia.